COBEM 2023 27TH INTERNATIONAL CONGRESS OF MECHANICAL ENGENEERING

ABCM Brazilian Society of Mechanical Sciences and Engineering
27th ABCM International Congress of Mechanical Engineering
December 04-08, 2023, Florianópolis-SC, Brazil

COB-2023-1067
INVESTIGATION OF A NOVEL METASTRUCTURE WITH TRAPPED, FLUID-FILLED UNIT CELLS

Vinícius Mauro de Souza Santos
Thiago de Paula Sales
Aeronautics Institute of Technology, Pç. Mal. Eduardo Gomes, 50 – Vila das Acácias, São José dos Campos, SP, Brazil
vinicius.santos@ga.ita.br, tpsales@ita.br

Morvan Ouisse
SUPMICROTECH, Université de Franche-Comté, CNRS, Institut FEMTO-ST, F-25000 Besançon, France
morvan.ouisse@femto-st.fr

Abstract. *The interaction between fluid and structure has long been a subject of interest in various engineering disciplines. Recently, microporous-like periodic structures with entrained fluid have demonstrated remarkable wave propagation properties, offering potential for designing versatile metamaterials. In this study, a novel metamaterial concept is proposed and investigated using the Wave-based Finite Element Method (WFEM). The metamaterial comprises a periodic-like structure manufactured through fused filament deposition, featuring internal cavities filled with water. Experimental characterization of the dynamics of the periodic system without internal fluid confirms good agreement with numerical predictions, obtained through frequency response function measurements. Furthermore, the dynamic behavior of the two-phase periodic metastructure is experimentally examined, where waves interact within the heterogeneous medium consisting of both fluid and solid phases. In this case, the resulting wave characteristics depend on the properties of both phases. It was shown that the fluid-filled metastructure exhibits a significantly wider bandgap compared to the periodic system lacking internal fluid, owing to the system's periodicity, mass increasing, and damping effects. Consequently, this work presents a promising avenue for metastructure design, with potential applications in structural dynamics and acoustics.*

Keywords: *metamaterial, bandgap, periodic structures, fluid-structure interaction, wave-based finite element method*

1. INTRODUCTION

The study of periodic and quasi-periodic structures opened possibilities to explore several properties that are not naturally encountered in nature: waveguiding (Pal and Ruzzene, 2017), bandgap formation (Wang *et al.*, 2019), confinement and mode localization phenomena (Wu *et al.*, 2009), invisibility cloaks (Ning *et al.*, 2020), mode conversion (Wang *et al.*, 2016), and some negative equivalent properties such as refractive index, elastic modulus, and Poisson's ratio (Gao *et al.*, 2022). Such structures are usually referred to as metastructures just because they can exhibit apparent properties, as listed earlier, which are not typically observed in conventional systems. However, there are certain instances in nature where periodicity can be found, such as in forests that behave as large-scale natural metamaterials, exhibiting unusual properties related to wave propagation (Liu *et al.*, 2019). Probably, in the context of structural dynamics, the most studied phenomenon related to periodic structures is what one knows as a bandgap, which comprises a frequency range where only evanescent wavemodes are allowed to occur (Miranda *et al.*, 2019). This phenomenon can arise from Bragg-scattering (Nobrega *et al.*, 2016), periodic arrangements of resonators within a host structure (Deng *et al.*, 2022), or specially designed unit cells incorporating inertial amplification mechanisms (IAMs) (Mizukami *et al.*, 2021).

In certain scenarios, both metastructures and conventional systems can exhibit complex dynamic behavior due to multiphysics problems. These may involve fluid-structure interaction (FSI), thermoelasticity, piezoelectric materials, magnetic forces, acoustic-structure interaction (ASI), viscoelasticity, and more. In this work, particular emphasis is placed on the dynamics of systems with enclosed fluid. The coupling of fluid dynamics with structural systems has been a longstanding concern in various fields, including structural engineering, aeroelasticity, hydroelasticity, vibroacoustics, wind engineering, ocean engineering, biomechanics, offshore engineering, aerospace engineering, and civil engineering. For instance, in previous research by Jamshidiat and SenGupta (1991), a method based on traditional finite element (FE) procedures was developed to predict the natural frequencies and modes of an aircraft fuselage considering the enclosed fluid medium. The approach involved establishing a structure-fluid interface area to couple the dynamics of the fuselage with the internal fluid. The stiffness and mass matrices of a representative unit cell of the structure were obtained from FE software, followed by establishing coupled structure-fluid equations in the frequency domain. By introducing a phase constant to account for end conditions and length, an eigenvalue problem was solved, enabling the computation of natural

frequencies and mode shapes that are reasonably close with analytical and Finite Element Method (FEM) results.

Although extensive research on FSI has been conducted in the aforementioned fields, it is crucial to consider the dynamics of metamaterials interacting with acoustic fluids. One notable investigation by Spadoni *et al.* (2014) focused on studying the dynamic behavior of closed-cell crystalline foams to explore the potential of these relatively few explored metamaterials. The complex microstructure of closed-cell crystalline foams, as highlighted by Spadoni *et al.* (2014), inherently possesses internal resonances, facilitating local resonance phenomena. Through a classical vibroacoustic model, Spadoni *et al.* (2014) demonstrated that truncated-octahedron (or Kelvin foam), face-centered cubic rhombic dodecahedron, and Weaire-Phelan foams exhibit superanisotropic properties, capable of behaving selectively as either a fluid or a solid. These foams display pentamode characteristics and feature regimes characterized by film resonances and a high density of states. These extraordinary properties can find effective utilization in various engineering and scientific disciplines, such as aerospace engineering, civil engineering, mechanical engineering, and acoustics, particularly in the design of metamaterials for specific purposes. The study also revealed the existence of persistent modes, which remain unaffected by the presence or absence of an entrained acoustic fluid. Furthermore, it was observed that the propagating shear modes, away from film resonances, are persistent modes, suggesting the hydrostatic behavior of the fluid-filled unit cell — in this case, the fluid does not influence the volumetric deformations of the foam.

Dorodnitsyn and Damme (2016) introduced and experimentally investigated a novel acoustic metamaterial incorporating an entrained fluid. The authors highlighted the interaction between waves traveling through the combined media, consisting of both fluid and solid components, which leads to coupled elastic waves with dynamics influenced by both phases. Notably, the acoustic metamaterial studied by Dorodnitsyn and Damme (2016) exhibits a negative refractive index behavior, owing to the opposite signs of the system's group and phase velocity. The experimental results presented by Dorodnitsyn and Damme (2016) substantiated numerical findings from prior studies regarding the shearing mode shapes, group velocity, and location of bandgaps. In addition, this research has opened up a new and straightforward pathway for designing acoustic metamaterials with exceptional properties not readily found in nature. These findings hold promise for various practical engineering applications and contribute to the vibroacoustic community.

Most of the time, analytical expressions are employed with the aim to model the aforementioned FSI problems. However, it is well known that these expressions are limited to approximate theories, and as a result, the established models are valid only under certain specific conditions. One cannot leave mentioning that the majority of analytical models in FSI typically represent simple systems, such as fluid-filled shells. In addition, mainly seminal works published in the fifties and sixties have been focused on wave propagation behavior in empty and fluid-filled cylindrical shells with real wavenumbers, which may not accurately reflect various practical conditions (Mirsky and Herrmann, 1957; McNiven *et al.*, 1966).

In an attempt to address some of the limitations discussed previously, Bao *et al.* (2000) presented closed-form expressions and conducted a theoretical study on dispersion curves of empty and fluid-filled cylindrical shells under axially symmetric waves, relying on Bessel functions, based on expressions derived by Kumar and Stephens (1972). Parametric analyses considering the wall thickness of both empty and fluid-filled systems were performed, yielding results similar to those obtained by Kumar and Stephens (1972). In summary, Bao *et al.* (2000) demonstrated that dispersion curves of such cylindrical shells can exhibit purely real, purely imaginary, and complex branches. The degree of coupling between the internal fluid and the shell was found to be strongly influenced by the shell thickness. Furthermore, it was observed that the internal fluid could considerably alter the wave propagation characteristics of the cylindrical shell. It has the ability to shift the cut-off frequencies of the wavemodes, providing a valuable means to control the dynamics of a metamaterial, which was not discussed at that time. Moreover, Bao *et al.* (2000) emphasized that certain branches seen in the dispersion curve of the fluid-filled cylindrical shell arise exclusively due to the presence of the fluid and may be purely evanescent. This realization suggests that fluid-filled systems can be exploited as a strategy for designing specially engineered structures with outstanding vibration attenuation performance for those pursuing such goals.

Fuller and Fahy (1982) derived closed-form expressions to predict the characteristics of elastic and acoustic wave propagation in a cylindrical elastic shell filled with fluid. The authors highlighted that when two fields, such as structural and acoustic, are coupled, the resulting wave behavior becomes complex. They demonstrated that when a cylindrical shell is filled with fluid, a fluid loading term, arising from the presence of the fluid acoustic field, must be considered in the system's free vibration. This term, however, does not exist in vacuum cylindrical shells for obvious reasons. Consequently, the authors showed that the magnitude of the fluid loading term can vary greatly, determining the level of coupling between the shell and the fluid. Furthermore, Fuller and Fahy (1982) conducted several parametric analyses considering factors such as wall thickness and the density ratio between the shell material and the internal fluid, that provide valuable insights into the dynamics of more complex fluid-filled systems. The same study also developed an expression for energy distribution, indicating that the concentration of energy can be in either the fluid or the shell wall, depending on the excitation frequency.

As seen before, earlier studies have effectively formulated analytical expressions to comprehend wave propagation in fluid-filled elastic pipes, despite their inherent simplifications. These expressions often provide a clearer and easier interpretation of wave propagation phenomena compared to numerical methods. However, as discussed previously, it is widely recognized that analytical solutions have limitations, as they are constrained to simple geometries and classical

wave theories. They are also constrained to a narrow range of vibroacoustic problems due to the complicated interaction that may occur between the acoustic fluid and the structure. To address these limitations, Mencik and Ichchou (2007) presented a general formulation using the Wave-based Finite Element Method (WFEM), in which the governing elasto-acoustic equations are discretized using the FEM, and the problem is formulated and solved in the wave space. The authors showed two mathematical strategies for handling fluid-filled structure problems: the (**U**, **p**) and (**U**, **Ψ**) formulations. In the first approach, the equations of motion for the acoustic fluid and the structure depend on the acoustic pressures of the fluid (**p**) and the structural degrees of freedom (**U**), resulting in an asymmetrical set of equations of motion. On the other hand, the second approach is a new version of the (**U**, **p**) formulation that introduces the acoustic velocity potential **Ψ** to formulate the elasto-acoustic problem symmetrically. The authors demonstrated the robustness of their numerical approach compared to analytical formulations, such as the one presented in (Fuller and Fahy, 1982). It was confirmed that the simplifying assumptions used in the analytical formulation are not entirely adequate and may hinder the accurate assessment of the system's dynamic behavior. However, several findings from Fuller and Fahy (1982) were confirmed by the numerical model presented by Mencik and Ichchou (2007).

Numerical methods, including the WFEM, have strengths and weaknesses in engineering applications. Challenges can arise when applying the WFEM to composite structures and FSI problems. In such cases, a fine unit cell mesh is required to accurately capture the structural dynamics. A coarse unit cell mesh can fail to predict the eigenvalues and eigenvectors related to the wave propagation characteristics throughout the system. Droz *et al.* (2014) addressed this issue and provided a brief review of free wave propagation in one-dimensional waveguides using the WFEM. To improve computational efficiency compared to traditional FEM, the authors proposed a model reduction strategy that utilized a reduced basis to model the structural dynamic behavior. Cut-on frequencies were identified within the analyzed frequency band, which allowed for the solution of a low-order modified eigenvalue problem for these frequencies. The eigenvectors associated with propagating waves (for which the real part of the wavenumber is much greater than its imaginary part) are chosen to form the reduced basis, using an iterative scheme to avoid redundant wave shapes. After building the optimized basis, a reduced eigenvalue problem, with size dependent on the number of propagating waves in the analyzed frequency range, is solved. The proposed methodology was validated through a three-layered sandwich beam, and an elastic pipe filled with acoustic fluid. Additionally, Mencik (2018) also presented a valuable way to increase the computational efficiency of the WFEM, based on the Craig-Bampton (CB) model order reduction technique.

From this literature review, which showed various modeling strategies for addressing FSI problems, and also highlighted promising applications of FSI in the dynamics of metamaterials, this study aims to propose a novel concept of metamaterial with completely closed unit cells filled with water, as depicted in Fig. 1. In this illustration, the metastructure consists of six identical unit cells, with the internal cavity represented by the blue color indicating the confined water. Firstly, a numerical model of the system without internal fluid is developed using the WFEM. Based on the Bloch-Floquet theorem and the matrices provided by the FEM, dispersion curves for the underlying unit cell are computed. Experimental FRFs for longitudinal and bending dynamics, obtained through hammer tests, are also made available and compared with numerical predictions. Subsequently, the dynamic behavior of the proposed fluid-filled metastructure is experimentally evaluated in order to gain a comprehensive understanding of its dynamic characteristics. This later realization enables the design of structures with exceptional wave absorption performance and passive vibration attenuation.

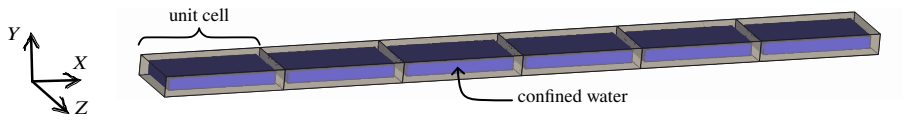

Figure 1: A periodic metastructure filled with water fluid, consisting of six identical unit cells.

Beyond this introduction, this work has been divided into five sections. First, in Section 2 we review the WFEM, which can be used to model the fluid-filled metastructure shown in Fig. 1. Dispersion curves, numerical and experimental FRFs are shown in Section 3. Discussions about the dynamics of the system with and without fluid are supplied, as well. A summary of our findings and conclusions is given in Section 4. Acknowledgments and references are provided at last.

2. MODELING

Assume that one unit cell of the periodic structure portrayed in Fig. 1 is meshed employing three-dimensional FEs, taking into account the fluid and solid behavior. Their corresponding mass and stiffness matrices are then extracted from conventional FE software, and by considering fluid and structural damping effects, one can write (Mencik and Ichchou, 2007):

$$\hat{\mathbf{M}}\ddot{\hat{\mathbf{q}}} + \hat{\mathbf{C}}\dot{\hat{\mathbf{q}}} + \hat{\mathbf{K}}\hat{\mathbf{q}} = \hat{\mathbf{F}}, \tag{1}$$

where $(\dot{\ })$ represents derivatives with respect to time and:

$$\hat{\mathbf{M}} = \begin{bmatrix} \mathbf{M}_\mathrm{S} & \mathbf{0} \\ \rho\,\mathbf{R}^\mathrm{T} & \mathbf{M}_\mathrm{A} \end{bmatrix}, \qquad \hat{\mathbf{C}} = \begin{bmatrix} \mathbf{C}_\mathrm{S} & \mathbf{0} \\ \mathbf{0} & \mathbf{C}_\mathrm{A} \end{bmatrix}, \qquad \hat{\mathbf{K}} = \begin{bmatrix} \mathbf{K}_\mathrm{S} & -\mathbf{R} \\ \mathbf{0} & \mathbf{K}_\mathrm{A} \end{bmatrix}, \qquad \hat{\mathbf{q}} = \begin{Bmatrix} \hat{\mathbf{U}} \\ \hat{\mathbf{p}} \end{Bmatrix}, \qquad \hat{\mathbf{F}} = \begin{Bmatrix} \hat{\mathbf{F}}_\mathrm{S} \\ \hat{\mathbf{F}}_\mathrm{A} \end{Bmatrix}. \tag{2}$$

In the two previous equations, $\mathbf{M}_j$, $\mathbf{C}_j$, and $\mathbf{K}_j$ ($j \in \{\mathrm{S},\ \mathrm{A}\}$) stand for mass, damping and stiffness matrices of structure (S) and acoustic-fluid (A) parts; $\mathbf{R}$ stands for the fluid-structure coupling matrix; $\ddot{\hat{\mathbf{U}}}$, $\dot{\hat{\mathbf{U}}}$, $\hat{\mathbf{U}}$, and $\hat{\mathbf{F}}_\mathrm{S}$ are acceleration, velocity, displacement, and load vectors of the structure domain; $\ddot{\hat{\mathbf{p}}}$, $\dot{\hat{\mathbf{p}}}$, $\hat{\mathbf{p}}$, and $\hat{\mathbf{F}}_\mathrm{A}$ are acceleration, velocity, displacement, and load vectors related to the internal fluid; ρ is the fluid density; and $(\ .\ )^\mathrm{T}$ is the transpose operator.

As discussed in Section 1, the use of WFEM may become a challenge in some certain conditions where a high number of internal degrees of freedom (DoFs) is found. To overcome this computational trouble, DoFs that are not located in the unit cell's left (L) and right (R) interfaces, namely internal (I), can be reduced employing the CB model order reduction method. The procedure, basically, consists of establish the following transformation matrix:

$$\boldsymbol{\alpha} = \begin{bmatrix} \mathbf{I} & \mathbf{0} \\ \boldsymbol{\Phi}_\mathrm{C} & \boldsymbol{\Phi}_\mathrm{N} \end{bmatrix}, \tag{3}$$

where $\mathbf{I}$ is an identity matrix, $\boldsymbol{\Phi}_\mathrm{C} = \hat{\mathbf{K}}_\mathrm{II}^{-1}\hat{\mathbf{K}}_\mathrm{IB}$ (B accounts for boundary DoFs comprising those located in both left and right interfaces), and $\boldsymbol{\Phi}_\mathrm{N}$ is a matrix of eigenvectors obtained from an eigenproblem that represents the dynamics of the considered unit cell with boundary DoFs constrained (Mencik, 2018). Since $\hat{\mathbf{q}} = \boldsymbol{\alpha}\mathbf{q}$, the reduced set of equations of motion can be written as:

$$\mathbf{M}\ddot{\mathbf{q}} + \mathbf{C}\dot{\mathbf{q}} + \mathbf{K}\mathbf{q} = \mathbf{F}, \qquad \text{with} \qquad \mathbf{M} = \boldsymbol{\alpha}^\mathrm{T}\hat{\mathbf{M}}\boldsymbol{\alpha}, \qquad \mathbf{C} = \boldsymbol{\alpha}^\mathrm{T}\hat{\mathbf{C}}\boldsymbol{\alpha}, \qquad \mathbf{K} = \boldsymbol{\alpha}^\mathrm{T}\hat{\mathbf{K}}\boldsymbol{\alpha}, \qquad \text{and} \qquad \mathbf{F} = \boldsymbol{\alpha}^\mathrm{T}\hat{\mathbf{F}}. \tag{4}$$

It is worth noting that a modified version of the previously mentioned model reduction methodology might be employed to address structural systems interacting with enclosed acoustic fluids, as discussed elsewhere (Maess and Gaul, 2006).

The reduced coupled fluid-structure equations seen before in Eq. (4) can be rewritten in the frequency domain, considering the $(\mathbf{U}, \mathbf{p})$ formulation, i.e., $\mathbf{D}\mathbf{q} = \mathbf{F}$, where $\mathbf{D} = -\omega^2\mathbf{M} + \mathrm{i}\omega\mathbf{C} + \mathbf{K}$, i is the imaginary unit, and ω is the circular frequency (Mencik and Ichchou, 2007). Following the basic procedure of the WFEM, the reduced DoFs and load vectors can be explicitly organized with respect to their position in the unit cell:

$$\begin{bmatrix} \mathbf{D}_\mathrm{LL} & \mathbf{D}_\mathrm{LR} & \mathbf{D}_\mathrm{LI} \\ \mathbf{D}_\mathrm{RL} & \mathbf{D}_\mathrm{RR} & \mathbf{D}_\mathrm{RI} \\ \mathbf{D}_\mathrm{IL} & \mathbf{D}_\mathrm{IR} & \mathbf{D}_\mathrm{II} \end{bmatrix} \begin{Bmatrix} \mathbf{q}_\mathrm{L} \\ \mathbf{q}_\mathrm{R} \\ \mathbf{q}_\mathrm{I} \end{Bmatrix} = \begin{Bmatrix} \mathbf{F}_\mathrm{L} \\ \mathbf{F}_\mathrm{R} \\ \mathbf{F}_\mathrm{I} \end{Bmatrix}, \tag{5}$$

which may be used to obtain an expression that relates DoFs and load vectors of the left interface between two adjacent unit cells of a periodic structure, the $(n+1)$ and (n), i.e., $\mathbf{u}_\mathrm{L}^{(n+1)} = \mathbf{S}\mathbf{u}_\mathrm{L}^{(n)} + \mathbf{b}^{(n)}$. This recurrence relation incorporates the unit cells' state vector $\mathbf{u}_\mathrm{L} = \{\mathbf{q}_\mathrm{L}^\mathrm{T}\ \mathbf{F}_\mathrm{L}^\mathrm{T}\}^\mathrm{T}$, a transfer matrix $\mathbf{S}$, and a forcing vector related to external loads $\mathbf{b}$ (Hoang *et al.*, 2020).

Bloch-Floquet theorem can be resorted to, so that the recurrence relation stated before leads to $(\mathbf{S} - \mu_j\mathbf{I})\boldsymbol{\phi}_j = \mathbf{0}$. Here, μ_j and $\boldsymbol{\phi}_j$ ($j \in \{1, ..., 2n_b\}$), being n_b the number of DoFs in the left (or right) interface of the unit cell, are eigensolutions (wavemodes) of the transfer matrix eigenproblem that physically represent the propagation constant and wave shapes, respectively. Wavenumbers can be computed from propagation constants as $k_j = (\ln\mu_j)/(-\mathrm{i}\Delta)$, where Δ is the length of the unit cell along the direction of wave propagation — assumed to be in the X-direction, cf. Fig. 1. As discussed by Waki *et al.* (2009b) and Mencik (2014), the standard eigenvalue problem described earlier may be prone to numerical issues due to ill-conditioning problems. Thus, to alleviate potential computational challenges one can resort to the alternative formulation $(\mathbf{N}\mathbf{J}\mathbf{L}^\mathrm{T} + \mathbf{L}\mathbf{J}\mathbf{N}^\mathrm{T} - \lambda_j\mathbf{L}\mathbf{J}\mathbf{L}^\mathrm{T})\mathbf{z}_j = \mathbf{0}$ (Zhong and Williams, 1995), where λ_j and $\mathbf{z}_j$ are eigensolutions of the Zhong's eigenvalue problem — expressions for $\mathbf{N}$, $\mathbf{J}$, and $\mathbf{L}$ can be found in (Mencik and Duhamel, 2015). The set of wavemodes associated with the transfer matrix eigenvalue problem $(\mu_j,\ \boldsymbol{\phi}_j)$ can be retrieved from λ_j and $\mathbf{z}_j$, following the procedure outlined by Mencik and Duhamel (2015).

Wavemodes computed previously can be grouped with respect to the direction of wave propagation, i.e., in positive-$(\mu_j, \boldsymbol{\phi}_j)$ and negative-going waves $(\mu_j^*, \boldsymbol{\phi}_j^*)$ as follows (Duhamel *et al.*, 2006; Waki *et al.*, 2009a):

$$\boldsymbol{\mu} = \mathrm{diag}(\mu_1, \ldots, \mu_{n_b}), \quad \boldsymbol{\mu}^* = \mathrm{diag}(\mu_1^*, \ldots, \mu_{n_b}^*), \quad \boldsymbol{\Phi} = [\boldsymbol{\phi}_1 \ldots \boldsymbol{\phi}_{n_b}] = \begin{bmatrix} \boldsymbol{\Phi}_q \\ \boldsymbol{\Phi}_F \end{bmatrix}, \quad \boldsymbol{\Phi}^* = [\boldsymbol{\phi}_1^* \ldots \boldsymbol{\phi}_{n_b}^*] = \begin{bmatrix} \boldsymbol{\Phi}_q^* \\ \boldsymbol{\Phi}_F^* \end{bmatrix}, \tag{6}$$

with subscripts q and F used to denote partitions of the wave shapes related to DoFs and loads, respectively. To develop expressions presented afterward, one highlights that eigenvectors must be normalized as described in (Mencik, 2014). In addition, since the wavemodes are computed for each desired frequency independently, some frequency tracking procedure might be used to better visualize dispersion curves, i.e., the relation between wavenumbers and frequency. Given a pair

of wavemodes related to eigenvalues μ_a and μ_a^*, with $\mu_a = 1/\mu_a^*$, the wavemode corresponding to μ_a at the consecutive frequency $\omega + \delta_\omega$ is chosen so that (Mencik, 2010):

$$\left| \frac{\boldsymbol{\phi}_a^{*\mathrm{T}}(\omega)}{||\boldsymbol{\phi}_a^*(\omega)||} \mathbf{J} \frac{\boldsymbol{\phi}_a(\omega+\delta_\omega)}{||\boldsymbol{\phi}_a(\omega+\delta_\omega)||} \right| = \max_{b \in \{1,\ldots,n_b\}} \left\{ \left| \frac{\boldsymbol{\phi}_a^{*\mathrm{T}}(\omega)}{||\boldsymbol{\phi}_a^*(\omega)||} \mathbf{J} \frac{\boldsymbol{\phi}_b(\omega+\delta_\omega)}{||\boldsymbol{\phi}_b(\omega+\delta_\omega)||} \right| \right\}, \tag{7}$$

where $||\ \ ||$ denotes the norm of a vector, and $|\ \ |$ denotes the absolute value of a scalar.

Lastly, the forced response of a finite structure with N unit cells can be calculated using the following expressions (Hoang *et al.*, 2020):

$$\mathbf{q}_{\mathrm{L}}^{(n)} = \boldsymbol{\Phi}_q \boldsymbol{\mu}^{n-1} \mathbf{Q} + \boldsymbol{\Phi}_q^* \boldsymbol{\mu}^{N+1-n} \mathbf{Q}^* + \boldsymbol{\Phi}_q \sum_{k=1}^{n-1} \boldsymbol{\mu}^{n-k-1} \mathbf{Q}_B^{(k)} - \boldsymbol{\Phi}_q^* \sum_{k=n}^{N} \boldsymbol{\mu}^{k+1-n} \mathbf{Q}_B^{*(k)}, \tag{8}$$

$$-\mathbf{F}_{\mathrm{L}}^{(n)} = \boldsymbol{\Phi}_F \boldsymbol{\mu}^{n-1} \mathbf{Q} + \boldsymbol{\Phi}_F^* \boldsymbol{\mu}^{N+1-n} \mathbf{Q}^* + \boldsymbol{\Phi}_F \sum_{k=1}^{n-1} \boldsymbol{\mu}^{n-k-1} \mathbf{Q}_B^{(k)} - \boldsymbol{\Phi}_F^* \sum_{k=n}^{N} \boldsymbol{\mu}^{k+1-n} \mathbf{Q}_B^{*(k)}, \tag{9}$$

being $\mathbf{Q}_B^{(k)}$ and $\mathbf{Q}_B^{*(k)}$ wavemode amplitudes related to externally applied loads; $\mathbf{Q} \equiv \mathbf{Q}^{(1)}$ and $\mathbf{Q}^* \equiv \mathbf{Q}^{*(N+1)}$ wavemode amplitudes for the first (1) and $(N+1)$ unit cell of the considered finite structure. It should be stressed that when the interaction between fluid and structure is taken into account, the equations of motion of the unit cell are unsymmetrical. Therefore, expressions for $\mathbf{Q}_B^{(k)}$ and $\mathbf{Q}_B^{*(k)}$ provided by Hoang *et al.* (2020) must be rewritten accordingly. In light of this, Eqs. (8) and (9) can be used to enforce boundary conditions and establish a linear system of equations for the unknowns $\mathbf{Q}$ and $\mathbf{Q}^*$. Solving this system enables the determination of any response of the periodic structure. For the sake of clarity, in our case, aiming to simulate a free-free condition, $\mathbf{F}_{\mathrm{L}}^{(1)} = \mathbf{0}$ and $\mathbf{F}_{\mathrm{L}}^{(N+1)} = \mathbf{0}$ must be written, so that one obtains:

$$\begin{bmatrix} \mathbf{I} & \boldsymbol{\Phi}_F^{-1} \boldsymbol{\Phi}_F^* \boldsymbol{\mu}^N \\ \boldsymbol{\Phi}_F^{*-1} \boldsymbol{\Phi}_F \boldsymbol{\mu}^N & \mathbf{I} \end{bmatrix} \begin{Bmatrix} \mathbf{Q} \\ \mathbf{Q}^* \end{Bmatrix} = \begin{Bmatrix} \boldsymbol{\Phi}_F^{-1} \boldsymbol{\Phi}_F^* \sum_{k=1}^{N} \boldsymbol{\mu}^k \mathbf{Q}_B^{*(k)} \\ -\boldsymbol{\Phi}_F^{*-1} \boldsymbol{\Phi}_F \sum_{k=1}^{N} \boldsymbol{\mu}^{N-k} \mathbf{Q}_B^{(k)} \end{Bmatrix}. \tag{10}$$

3. EXPERIMENTAL AND NUMERICAL RESULTS

In the following sections, experimental and numerical results will be presented against with experimental procedures we employed. Firstly, discussions regarding the manufacture of the periodic structure and the FE model of its unit cell are provided in Section 3.1. A comparison between numerical and experimental findings are supplied in Section 3.2.

3.1. Manufacturing considerations and finite element model

The three-dimensional system examined in this study consists of unit cells constructed with an external parallelepiped with dimensions of $60 \times 10 \times 30$ mm^3 ($\Delta = 60$ mm), containing a perfectly centered internal void measuring $53.6 \times 6 \times 23.6$ mm^3. The numerical and experimental analyses presented here initially focus on the dynamic behavior of the periodic metastructure illustrated in Fig. 1, without internal fluid. A three-dimensional model of the system was created using computer-aided engineering (CAD) software and was subsequently made in separate parts using additive manufacturing, as depicted in Fig. 2a. Due to manufacturing limitations, the base of the periodic structure was printed first, resulting in the configuration depicted in Fig. 2b. Subsequently, the closing cap was produced with a nominal thickness of 2 mm, incorporating a 0.1 mm gap in the X-direction and a 0.2 mm gap in the Z-direction, to facilitate the assembly procedure. This led to the geometry displayed in Fig. 2c. Finally, the closing cap was bonded to the base of the metastructure using cyanoacrylate superglue, completing the periodic system shown in Fig. 2d.

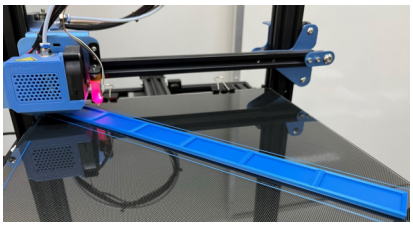

(a) Printing the base of the periodic metastructure using additive manufacturing.

(b) Base of the periodic metastructure.

(c) Closing cap of the periodic metastructure.

(d) Final assembled periodic metastructure after bonding its base with its closing cap.

Figure 2: Manufacture details of the periodic metastructure with voids (without fluid) studied in this work.

To conduct numerical investigations on the previously depicted system, the terms appearing in the equations of motion for the unit cell, as shown in Eq. (1), are reduced to $\hat{\mathbf{M}} = \mathbf{M}_{\mathrm{S}}$, $\hat{\mathbf{C}} = \mathbf{C}_{\mathrm{S}}$, $\hat{\mathbf{K}} = \mathbf{K}_{\mathrm{S}}$, $\hat{\mathbf{q}} = \hat{\mathbf{U}}$, and $\hat{\mathbf{F}} = \hat{\mathbf{F}}_{\mathrm{S}}$. The mass and stiffness matrices mentioned earlier are obtained from conventional FE software, assuming linear elasticity and utilizing

the FE mesh illustrated in Fig. 3. Specifically, 4-noded tetrahedral elements with three DoFs per node are employed, i.e., encompassing translations in the X, Y, and Z-directions, cf. Fig. 1. Furthermore, the modeling of the unit cell incorporates a total of 75242 FEs, with an element size of 1 mm. This configuration ensures model convergence up to the maximum analyzed frequency of 5000 Hz. The external parallelepiped is made of polylactic acid (PLA), with an elastic modulus of 2.24 GPa, a density of 1052.6 kg m^{-3}, and a Poisson's ratio of 0.3. Viscous damping is not considered in this study ($\hat{\mathbf{C}} = \mathbf{0}$). However, dissipation effects in the system's forced responses are accounted for through hysteretic damping, where $\hat{\mathbf{K}} = (1 + \mathrm{i}\eta)\mathbf{K}_\mathrm{S}$, with η being the structural damping coefficient set to 2×10^{-2} (Renno and Mace, 2010). Moreover, a complete wave basis comprising 714 left- and right-going wavemodes (i.e., $n_b = 357$) was employed to characterize the dynamics of the unit cell under investigation. This choice was based on the demonstrated relevance of highly evanescent wavemodes in the dynamics of the system we are examining during numerical validations of the wave-based approach against FE analyses. Specifically, these evanescent wavemodes may be reflected by the internal boundaries near the excitation location and, therefore, should not be neglected when computing responses for a finite system with relatively small length. It is noteworthy that even when considering the complete wave basis to describe the behavior of the metastructure, one solves a significantly smaller linear system of equations compared to traditional FEM.

(a) Unit cell mesh. (b) Cut view revealing internal void and wall mesh.

Figure 3: Finite element mesh used to model the unit cells of the periodic metastructure shown in Fig. 1 without internal fluid by the Wave-based Finite Element Method.

3.2. Comparison between numerical and experimental results

First and foremost, the theory briefly discussed in Section 2 can be employed to calculate the dispersion curves for an infinite and undamped ($\eta = 0$) metastructure consisting of unit cells without internal fluid. Since the analyzed system does not exhibit any non-reciprocal properties in terms of wave propagation characteristics, the dispersion curves show symmetry with respect to the frequency axis. Therefore, Fig. 4 displays only the positive values of $\mathrm{Re}\{k_j\}$ and the corresponding negative values of $\mathrm{Im}\{k_j\}$ to visualize the dispersion curves. In Fig. 4, only the first four pairs of wavemodes that propagate (or spatially decay) to left and right directions were depicted, instead of all those 714 computed, for convenience. It is important to note that these wavemodes are related to propagating and evanescent modes and may be associated with longitudinal, bending, torsional, and shear wave types. Additionally, it is well-known that the mode behavior of some periodic structures can be frequency-dependent even for a single dispersion curve, necessitating a careful evaluation of each wave shape ($\boldsymbol{\phi}_j$) to accurately assess the wave behavior and dynamics. However, a detailed mode classification of each curve depicted in Fig. 4 is out of scope of this work. In spite of that, the focus here is on the wavemodes that most influence the longitudinal and bending dynamics in the X- and Y-directions, respectively, cf. Fig. 1. The dispersion curves corresponding to these particular modes are indicated in Fig. 4.

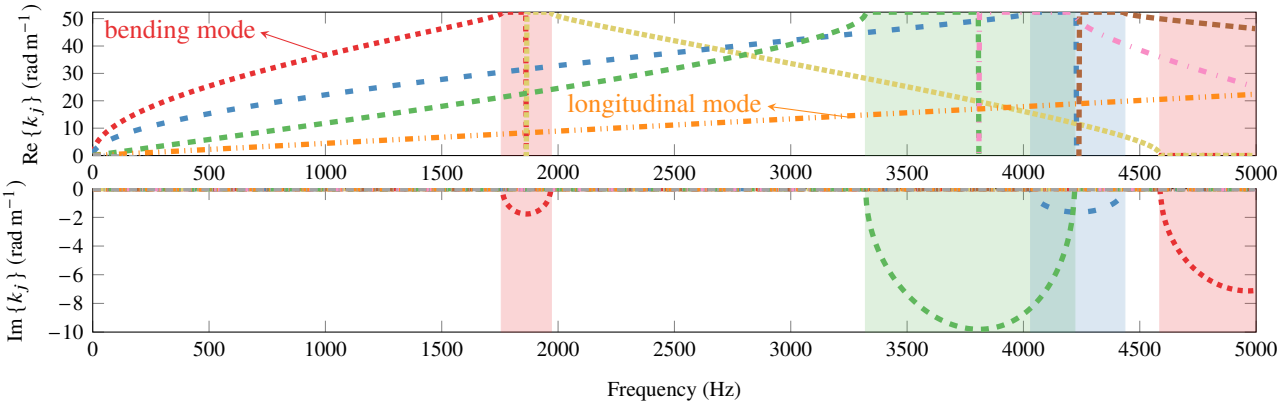

Figure 4: Dispersion curves (positive values of $\mathrm{Re}\{k_j\}$ and negative values of $\mathrm{Im}\{k_j\}$) and bandgaps frequency ranges ($\mathrm{Im}\{k_j\} \neq 0$) computed for the undamped ($\eta = 0$) unit cell of the periodic structure shown in Fig. 1, without fluid. The correspondence between wavenumbers depicted in $\mathrm{Re}\{k_j\}$ and $\mathrm{Im}\{k_j\}$ is illustrated by the dispersion curves with matching colors and line styles.

In addition to the dispersion curves shown in Fig. 4, bandgaps frequency ranges are also presented ($\mathrm{Im}\{k_j\} \neq 0$). To aid comprehension, these frequency bands are highlighted using shaded areas in colors that correspond to those used to plot the negative values of $\mathrm{Im}\{k_j\}$. Furthermore, to enhance clarity, a summary of these bandgap frequency ranges is provided in Table 1. Thus, based on the curves shown in Fig. 4 and the results provided in Table 1, it is evident that the investigated system exhibits four distinct forbidden zones up to 5 kHz.

Table 1: A summary of the bandgaps frequency ranges ($\mathrm{Im}\{k_j\} \neq 0$) seen in Fig. 4, computed for an undamped ($\eta = 0$) and infinite metastructure made with the unit cell shown in Fig. 1, without internal fluid.

Line-styles used in Fig. 4	Bandgap frequency ranges (Hz)
and	(1756 – 1971), (4586 – 5000)
and	(3321 – 4221)
and	(4031 – 4436)

To validate the previously observed numerical predictions regarding the wave behavior in a finite system consisting of $N = 6$ unit cells, cf. Fig. 2d, accelerance-type FRFs are measured in the longitudinal and transversal directions (X- and Y-directions, respectively). The experimental setups for these measurements are illustrated in Figs. 5a and 5b. For the investigation of the longitudinal behavior of the periodic system, the experimental scheme shown in Fig. 5a is utilized. An accelerometer PCB 352C22 was positioned at the left boundary of the system, while an impulsive force was applied at the right end. Both the input and output positions were located precisely at the center of the cross-section of the periodic structure. On the other hand, the bending behavior of the system was examined using the experimental setup depicted in Fig. 5b. In this case, the structure was spatially reoriented to minimize the influence of nylon strings on the free vibration of the system. Similar to Fig. 5a, the accelerometer was placed at the midpoint of the leftmost boundary, but in the XZ-plane. The hammer excitation force was applied in the same plane, at the rightmost edge, in the mid-line passing through the

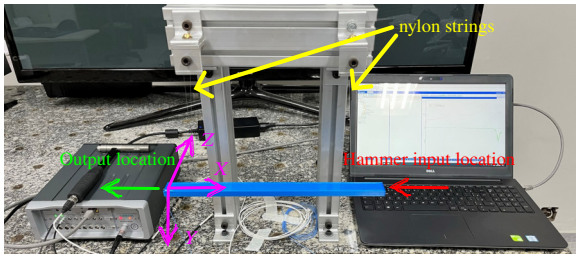

(a) Experimental setup used to investigate the longitudinal behavior of the periodic metastructure.

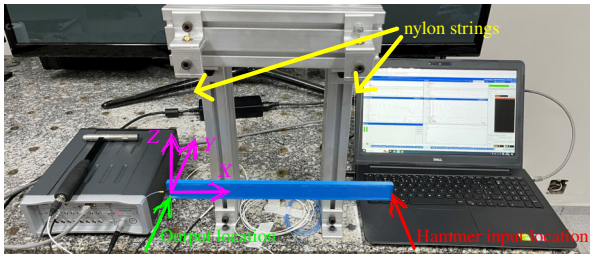

(b) Experimental setup used to investigate the bending behavior of the periodic metastructure.

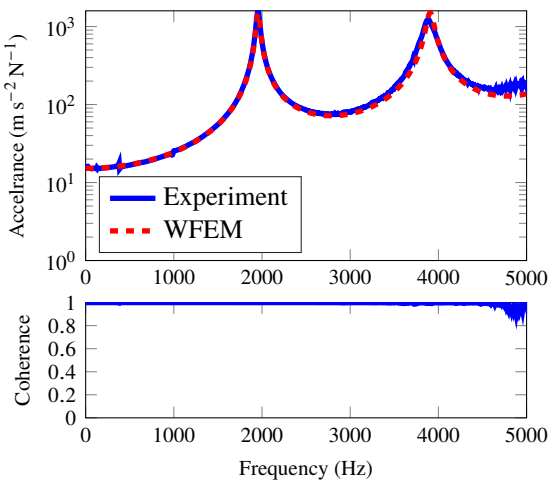

(c) A comparison between numerical and experimental FRFs corresponding to the input and output locations seen in Fig. 5a.

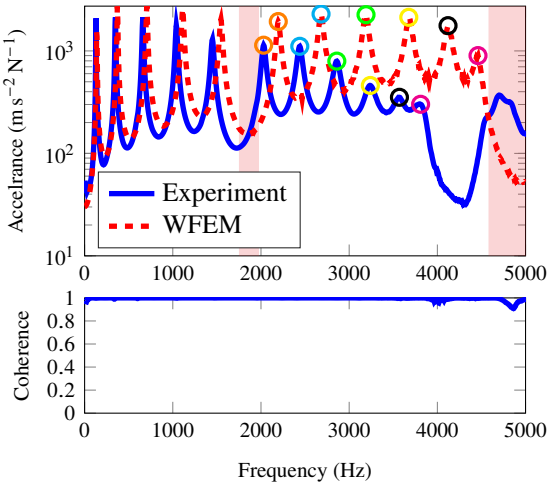

(d) A comparison between numerical and experimental FRFs corresponding to the input and output locations seen in Fig. 5b.

Figure 5: Experimental setups and comparisons between numerical and measured FRFs used to investigate the longitudinal and bending behavior of the periodic metastructure portrayed in Fig. 2d, without internal fluid.

XZ-plane. Accordingly, a comparison between numerical and experimental findings is presented in Figs. 5c and 5d for longitudinal and bending dynamics, respectively. It is important to note that numerical curves were computed using the wave-based theory discussed in Section 2, specifically by applying Eq. (8).

As one may notice from Fig. 5c, the numerical prediction match really well the experimental result obtained through the hammer test across the entire frequency range considered. Both resonance frequencies related to longitudinal motion of the system are accurately calculated, corresponding to approximately 1960 Hz and 3890 Hz. In addition, the experimental frequency ranges, far from the resonance condition, also exhibit strong agreement with the wave-based model. Moreover, the numerical predictions regarding the wave propagation behavior of longitudinal modes, provided by the Bloch-Floquet theorem as depicted in Fig. 4, are further supported by these FRFs. It means that the finite system did not experience attenuation zones in the considered frequency range regarding the propagation of longitudinal waves, since the dispersion curve seen in Fig. 4, related to this kind of motion, is purely real. Lastly, the coherence function depicted in Fig. 5c confirms the quality of the experimental data, indicating well-conducted experiments.

On the other hand, a comparison between numerical and experimental results depicted in Fig. 5d reveals that the wave-based model does not accurately describe the bending motion of the periodic structure without fluid, even with its longitudinal dynamics being properly predicted, as shown by Fig. 5c. In fact, the natural frequencies computed using the WFEM are larger than those identified from experimental data, indicating that the model exhibits a stiffer behavior. However, it is noteworthy that the number of resonant peaks observed in the numerical results perfectly matches those related to experiments — cf. this indication in Fig. 5d. Furthermore, the predictions derived from the Bloch-Floquet theorem regarding the attenuation zone of bending modes are confirmed by the numerical FRF shown in Fig. 5d. This shows that the finite system exhibits two forbidden zones up to 5 kHz, as illustrated by the red shaded areas in Fig. 5d. These attenuation zones are close to the steep valleys related to the blue curve, potentially corresponding to the actual attenuation zone of the tested finite system. Nevertheless, the forbidden zones identified through experiments are slightly shifted to the left, as previously discussed regarding the natural frequencies. This frequency shift, clearly depicted in Fig. 5d, can be attributed mainly to our assumption of a linear, isotropic constitutive relationship for the material, which does not fully reflect the system's actual behavior. For instance, the material is known to exhibit viscoelastic behavior (Müller *et al.*, 2022), and the 3D printing process we employed favors the resulting media to possess orthotropic symmetry (Torre and Brischetto, 2022). Notwithstanding, we chose to consider a linear model for our analysis, which still yields a good match with the experimental data. It is also worth mentioning that the coherence function associated with the bending-type motion test is good, similar to the results shown in Fig. 5c, indicating well-conducted experiments.

In order to experimentally assess the dynamic behavior of the system depicted in Fig. 2d, with unit cells completely filled with water, new experiments were conducted. Firstly, another periodic structure was manufactured, following the procedures described in Section 3.1. The surfaces of the six-cell periodic system that could potentially come into contact with water were sealed using varnish, to waterproof the prototype model obtained through additive manufacturing. Subsequently, the internal cavities were filled with fluid, and the closing cap was glued to the superior part of the base of the periodic structure. By adopting the same experimental setups discussed earlier and shown in Figs. 5a and 5b, longitudinal and bending accelerance FRFs were measured employing hammer tests for the water-filled periodic structure. Associated results are depicted in Fig. 6. The same figure also includes the experimental FRFs obtained for the system

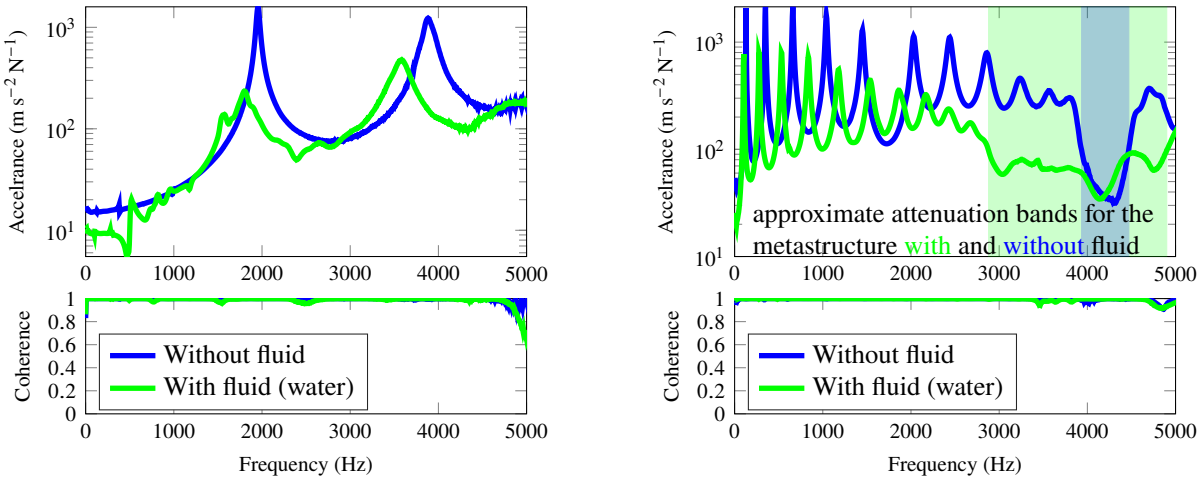

(a) Longitudinal accelerance FRFs corresponding to the input and output locations seen in Fig. 5a.

(b) Bending accelerance FRFs corresponding to the input and output locations seen in Fig. 5b.

Figure 6: A comparison between experimental FRFs measured for the periodic system portrayed in Fig. 2d, with and without internal fluid, to investigate its longitudinal and bending dynamic behavior.

without fluid, previously shown in Figs. 5c and 5d, for convenience and ease of comparison.

First, Figs. 6a and 6b show that most resonant peaks exist in both conditions when the system is without or completely filled with fluid. This observation was previously made by Spadoni *et al.* (2014) in their study on closed-cell crystalline foams, where these modes were referred to as persistent modes, cf. Section 1. In addition, a comparison between the blue and green curves depicted in Figs. 6a and 6b, reveals that the internal fluid significantly contributes to damping effects in the finite periodic system. This is evident from the noticeable attenuation of amplitudes at the frequencies corresponding to the system's resonance exhibited in the green curve in Fig. 6b. Turning attention to Fig. 6a, additional resonant frequencies emerge when the periodic system is filled with fluid. These frequencies may be associated with acoustic modes, requiring an examination of the system's deformed patterns at these frequencies to confirm this observation. Additionally, the results shown in Fig. 6b, related to bending dynamics, demonstrate that the region corresponding to the second experimental attenuation zone is significantly wider when the cavities are completely filled with water compared to the condition without internal fluid, as illustrated schematically using shading. This finding suggests a novel way to broad attenuation zones in metamaterials by leveraging the dynamic behavior of fluid-filled cells. Moreover, this realization confirms the outstanding performance of fluid-filled metamaterials in vibroacoustics, in terms of attenuating elastoacoustic waves.

4. CONCLUDING REMARKS

This study investigated the dynamic behavior of periodic structures with internal cavities completely filled with water and in absence of it. We reviewed a general formulation based on the WFEM to analyze the wave propagation phenomena in fluid-filled systems. Utilizing this wave-based modeling approach, simulations were conducted to investigate the dynamics of the periodic system without internal fluid. Additionally, dispersion curves were computed using the Bloch-Floquet theorem for the unit cell lacking fluid, providing insights into the wave propagation characteristics through the considered system. Experimental tests were conducted on a finite metastructure comprising six unit cells without fluid, and the measured accelerance FRFs exhibited good agreement with the predictions provided by the wave-based model. Furthermore, the attenuation zones predicted by the Bloch-Floquet theorem were confirmed in both the numerical and experimental accelerance responses. Moreover, the dynamic behavior of the metastructure made with fluid-filled unit cells was experimentally assessed through hammer tests. A comparison between the experimental FRFs of the regarded periodic structure without and with internal fluid revealed that the bandgap frequency range observed in the former case can be significantly enlarged in the presence of fluid within the unit cell's cavities. This indicates the potential of using such metamaterials as a novel passive vibration absorber mechanism in vibroacoustic engineering applications.

5. ACKNOWLEDGEMENTS

V. M. S. Santos acknowledges his doctorate scholarship by the Brazilian Coordination for the Improvement of Higher Education Personnel (CAPES). V. M. S. Santos and T. P. Sales are grateful to the São Paulo Research Foundation (FAPESP) for its support to the thematic grant #18/15894-0, related to the "Periodic structure design and optimization for enhanced vibroacoustic performance: ENVIBRO" research project. M. Ouisse acknowledges the graduate school EIPHI (project ANR-17-EURE-0002).

6. REFERENCES

Bao, X.L., Überall, H., Raju, P.K., Ahyi, A.C., Bjo/rno/, I.K. and Bjo/rno/, L., 2000. "Dispersion of axially symmetric waves in fluid-filled cylindrical shells". *J. Acoust. Soc. Am.*, Vol. 107, No. 5, pp. 2847–2848. doi:10.1121/1.429206.

Deng, J., Guasch, O., Maxit, L. and Gao, N., 2022. "A metamaterial consisting of an acoustic black hole plate with local resonators for broadband vibration reduction". *J. Sound Vib.*, Vol. 526, p. 116803. doi:10.1016/j.jsv.2022.116803.

Dorodnitsyn, V. and Damme, B.V., 2016. "Two-dimensional fluid-filled closed-cell cellular solid as an acoustic metamaterial with negative index". *Phys. Rev. B*, Vol. 93, No. 13, p. 134302. doi:10.1103/physrevb.93.134302.

Droz, C., Lainé, J.P., Ichchou, M.N. and Inquiété, G., 2014. "A reduced formulation for the free-wave propagation analysis in composite structures". *Compos. Struct.*, Vol. 113, pp. 134–144. doi:10.1016/j.compstruct.2014.03.017.

Duhamel, D., Mace, B.R. and Brennan, M.J., 2006. "Finite element analysis of the vibrations of waveguides and periodic structures". *J. Sound Vib.*, Vol. 294, No. 1-2, pp. 205–220. doi:10.1016/j.jsv.2005.11.014.

Fuller, C.R. and Fahy, F.J., 1982. "Characteristics of wave propagation and energy distributions in cylindrical elastic shells filled with fluid". *J. Sound Vib.*, Vol. 81, No. 4, pp. 501–518. doi:10.1016/0022-460x(82)90293-0.

Gao, N., Zhang, Z., Deng, J., Guo, X., Cheng, B. and Hou, H., 2022. "Acoustic Metamaterials for Noise Reduction: A Review". *Adv. Mater. Technol.*, Vol. 7, No. 6, p. 2100698. doi:10.1002/admt.202100698.

Hoang, T., Duhamel, D. and Foret, G., 2020. "Wave finite element method for waveguides and periodic structures subjected to arbitrary loads". *Finite Elem. Anal. Des.*, Vol. 179, p. 103437. doi:10.1016/j.finel.2020.103437.

Jamshidiat, H. and SenGupta, G., 1991. "Dynamics of periodic structures interacting with an enclosed fluid medium". *J. Sound Vib.*, Vol. 148, No. 1, pp. 103–115. doi:10.1016/0022-460x(91)90822-2.

Kumar, R. and Stephens, R.W.B., 1972. "Dispersion of flexural waves in circular cylindrical shells". *Proc. R. Soc. Lond. A.*, Vol. 329, No. 1578, pp. 283–297. doi:10.1098/rspa.1972.0114.

Liu, Y.F., kun Huang, J., Li, Y.G. and Shi, Z.F., 2019. "Trees as large-scale natural metamaterials for low-frequency vibration reduction". *Constr. Build. Mater.*, Vol. 199, pp. 737–745. doi:10.1016/j.conbuildmat.2018.12.062.

Maess, M. and Gaul, L., 2006. "Substructuring and model reduction of pipe components interacting with acoustic fluids". *Mech. Syst. Signal Pr.*, Vol. 20, No. 1, pp. 45–64. doi:10.1016/j.ymssp.2005.02.008.

McNiven, H.D., Sackman, J.L. and Shah, A.H., 1966. "Axially Symmetric Waves in Hollow, Elastic Rods. Part II". *J. Acoust. Soc. Am.*, Vol. 40, No. 5, pp. 1073–1076. doi:10.1121/1.1910190.

Mencik, J.M., 2010. "On the low- and mid-frequency forced response of elastic structures using wave finite elements with one-dimensional propagation". *Comput. Struct.*, Vol. 88, No. 11-12, pp. 674–689. doi:10.1016/j.compstruc.2010.02.006.

Mencik, J.M., 2014. "New advances in the forced response computation of periodic structures using the wave finite element (WFE) method". *Comput. Mech.*, Vol. 54, No. 3, pp. 789–801. doi:10.1007/s00466-014-1033-1.

Mencik, J.M. and Duhamel, D., 2015. "A wave-based model reduction technique for the description of the dynamic behavior of periodic structures involving arbitrary-shaped substructures and large-sized finite element models". *Finite Elem. Anal. Des.*, Vol. 101, pp. 1–14. doi:10.1016/j.finel.2015.03.003.

Mencik, J.M. and Ichchou, M.N., 2007. "Wave finite elements in guided elastodynamics with internal fluid". *Int. J. Solids Struct.*, Vol. 44, No. 7-8, pp. 2148–2167. doi:10.1016/j.ijsolstr.2006.06.048.

Mencik, J.M., 2018. "A wave finite element approach for the analysis of periodic structures with cyclic symmetry in dynamic substructuring". *J. Sound Vib.*, Vol. 431, pp. 441–457. doi:10.1016/j.jsv.2018.05.027.

Miranda, E.J.P., Nobrega, E.D., Ferreira, A.H.R. and Santos, J.M.C.D., 2019. "Flexural wave band gaps in a multi-resonator elastic metamaterial plate using Kirchhoff-Love theory". *Mech. Syst. Signal Pr.*, Vol. 116, pp. 480–504. doi:10.1016/j.ymssp.2018.06.059.

Mirsky, I. and Herrmann, G., 1957. "Nonaxially Symmetric Motions of Cylindrical Shells". *J. Acoust. Soc. Am.*, Vol. 29, No. 10, pp. 1116–1123. doi:10.1121/1.1908716.

Mizukami, K., Funaba, K. and Ogi, K., 2021. "Design and three-dimensional printing of carbon-fiber-composite elastic metamaterials with inertial amplification mechanisms". *J. Sound Vib.*, Vol. 513, p. 116412. doi:10.1016/j.jsv.2021.116412.

Müller, M., Šleger, V., Kolář, V., Hromasová, M., Piš, D. and Mishra, R.K., 2022. "Low-Cycle Fatigue Behavior of 3D-Printed PLA Reinforced with Natural Filler". *Polymers*, Vol. 14, No. 7, p. 1301. doi:10.3390/polym14071301.

Ning, L., Wang, Y.Z. and Wang, Y.S., 2020. "Active control cloak of the elastic wave metamaterial". *Int. J. Solids Struct.*, Vol. 202, pp. 126–135. doi:10.1016/j.ijsolstr.2020.06.009.

Nobrega, E.D., Gautier, F., Pelat, A. and Santos, J.M.C.D., 2016. "Vibration band gaps for elastic metamaterial rods using wave finite element method". *Mech. Syst. Signal Pr.*, Vol. 79, pp. 192–202. doi:10.1016/j.ymssp.2016.02.059.

Pal, R.K. and Ruzzene, M., 2017. "Edge waves in plates with resonators: an elastic analogue of the quantum valley Hall effect". *New J. Phys.*, Vol. 19, No. 2, p. 025001. doi:10.1088/1367-2630/aa56a2.

Renno, J.M. and Mace, B.R., 2010. "On the forced response of waveguides using the wave and finite element method". *J. Sound Vib.*, Vol. 329, No. 26, pp. 5474–5488. doi:10.1016/j.jsv.2010.07.009.

Spadoni, A., Höhler, R., Cohen-Addad, S. and Dorodnitsyn, V., 2014. "Closed-cell crystalline foams: Self-assembling, resonant metamaterials". *J. Acoust. Soc. Am.*, Vol. 135, No. 4, pp. 1692–1699. doi:10.1121/1.4867375.

Torre, R. and Brischetto, S., 2022. "Experimental characterization and finite element validation of orthotropic 3D-printed polymeric parts". *Int. J. Mech. Sci.*, Vol. 219, p. 107095. doi:10.1016/j.ijmecsci.2022.107095.

Waki, Y., Mace, B.R. and Brennan, M.J., 2009a. "Free and forced vibrations of a tyre using a wave/finite element approach". *J. Sound Vib.*, Vol. 323, No. 3-5, pp. 737–756. doi:10.1016/j.jsv.2009.01.006.

Waki, Y., Mace, B.R. and Brennan, M.J., 2009b. "Numerical issues concerning the wave and finite element method for free and forced vibrations of waveguides". *J. Sound Vib.*, Vol. 327, No. 1-2, pp. 92–108. doi:10.1016/j.jsv.2009.06.005.

Wang, H., Xu, Y., Genevet, P., Jiang, J.H. and Chen, H., 2016. "Broadband mode conversion via gradient index metamaterials". *Sci. Rep.*, Vol. 6, No. 1. doi:10.1038/srep24529.

Wang, K., Zhou, J., Wang, Q., Ouyang, H. and Xu, D., 2019. "Low-frequency band gaps in a metamaterial rod by negative-stiffness mechanisms: Design and experimental validation". *Appl. Phys. Lett.*, Vol. 114, No. 25, p. 251902. doi:10.1063/1.5099425.

Wu, T.C., Wu, T.T. and Hsu, J.C., 2009. "Waveguiding and frequency selection of Lamb waves in a plate with a periodic stubbed surface". *Phys. Rev. B*, Vol. 79, No. 10. doi:10.1103/physrevb.79.104306.

Zhong, W.X. and Williams, F.W., 1995. "On the direct solution of wave propagation for repetitive structures". *J. Sound Vib.*, Vol. 181, No. 3, pp. 485–501. doi:10.1006/jsvi.1995.0153.

7. RESPONSIBILITY NOTICE

The authors are solely responsible for the printed material included in this paper.